Global-local gyrokinetic simulations of turbulence in tokamak plasmas[1]

Denis St-Onge
Felix Parra and Michael Barnes

PPPL theory seminar

January 13, 2022

Engineering and Physical Sciences Research Council

[1]This work has been carried out within the framework of the EUROfusion Consortium and has received funding from the Euratom research and training programme 2014-2018 and 2019-2020 under Grant Agreement No. 633053, from the RCUK Energy Programme [Grant Number EP/P012450/1], and from the Engineering and Physical Sciences Research Council (EPSRC) [EP/R034737/1]. The views and opinions expressed herein do not necessarily reflect those of the European Commission.

Local (flux-tube) simulation

the good:

- ✓ spectral accuracy in the perpendicular dynamics
- ✓ gyro-averaging is simple
- ✓ typically fast

the bad:

- ✗ simple background profiles
- ✗ boundary conditions sensible only in a statistical sense
- ✗ can't describe non-local phenomena

Global simulation

the good:

- ✓ arbitrary profile variation
- ✓ non-local phenomena
- ✓ large-scale coherent structures

the bad:

- ✗ lose spectral accuracy in radial direction
- ✗ need to sweat a little to gyro-average
- ✗ Dirichlet BCs typical – intrinsic length-scale

Can we somehow marry these two approaches?

Two fundamental ideas to our approach:[1]

1. **Novel boundary conditions**

   Additional local flux-tube simulations are used to provide reasonable boundary conditions for global simulations.

2. **Subsidiary expansion of the gyrokinetic equation**

   By exploiting the large box sizes typical of flux-tube simulations, global effects can be incorporated as a next-order correction to the local ρ_*-small limit.

[1] Parra & Barnes, PPCF **57** (2015)

IDEA: Use additional flux-tube simulations at different radial locations to determine the boundary conditions in the 'main' simulation.

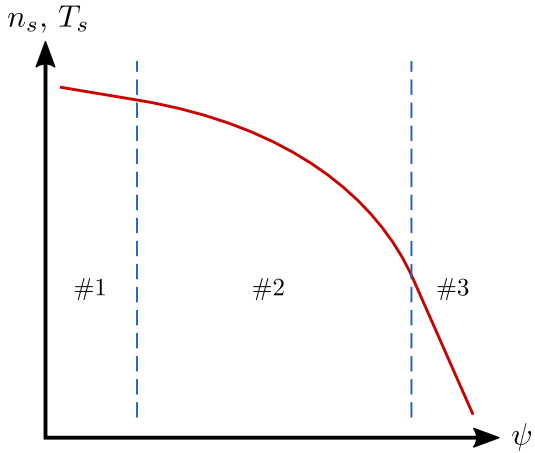

Figure: current implementation (parabolic)

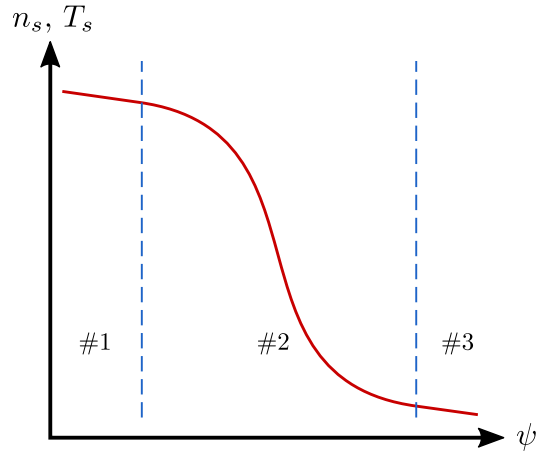

Figure: future implementation (arbitrary)

See Parra & Barnes, PPCF **57** (2015) for motivation.

Our global method has been implemented in the flux-tube code `stella`, which is freely available at the following link,

Link `https://github.com/stellaGK/stella`

Documentation on how to run `stella` will soon be available at

Link `https://stellagk.github.io/stella/`

For more details on `stella`, see Barnes *et al.* 2019 JCP. A preprint on global `stella` is now on the arXiv at

Link `https://arxiv.org/abs/2201.01506`

We have performed tests to ensure that our new approach has been implemented correctly and performs robustly.

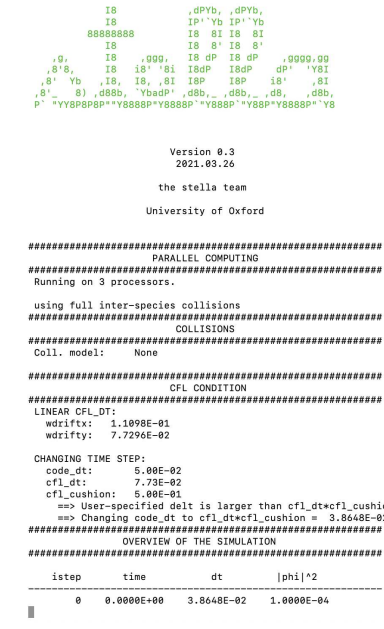

BOUNDARY CONDITION METHOD:

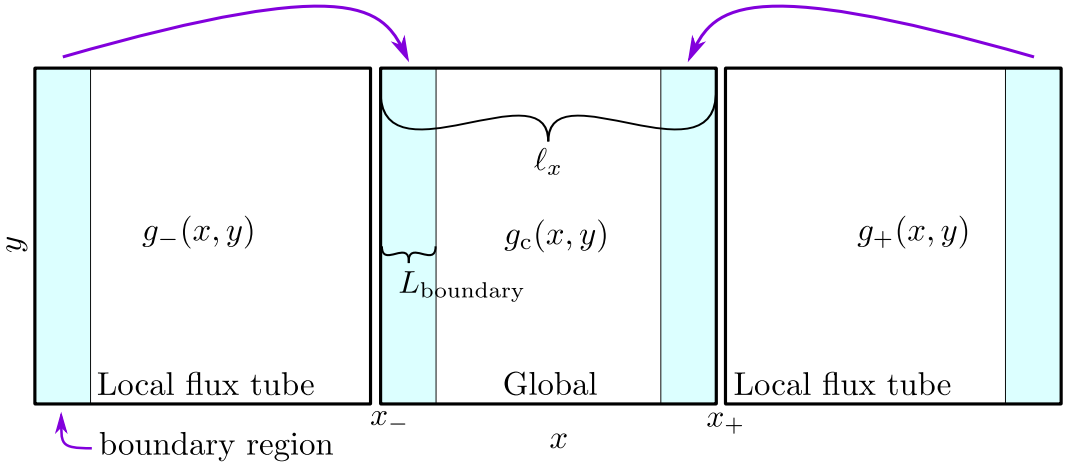

Figure: Illustration of our multiple-flux-tube method. Information about the distribution function g from two local and independent flux-tube simulations are fed into the boundary region of a central, 'global' simulation. See Candy *et al.* 2020 PPCF **62** 042001 for a complementary approach.

Simulations reveal excellent continuity between domains using the multibox approach with no radial profile variation:

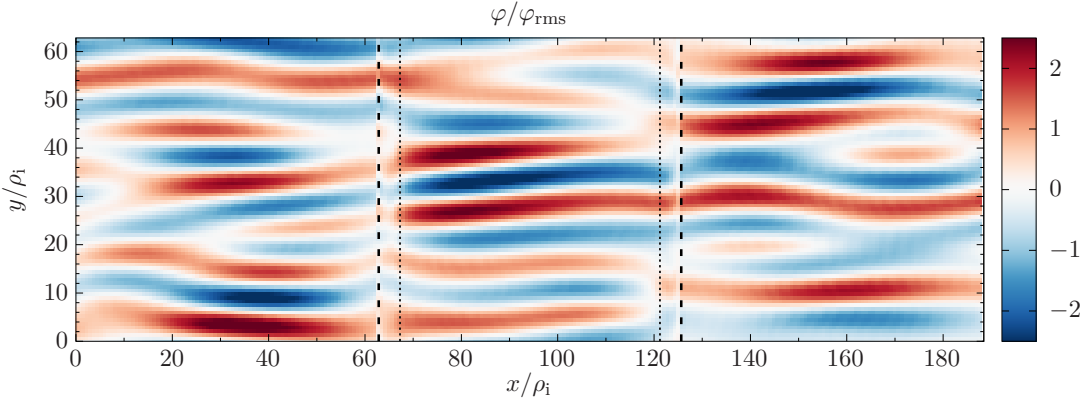

Figure: Electrostatic potential at the outboard midplane for the CBC using different initial conditions. Dashed lined indicate domain boundaries.

Simulations reveal excellent continuity between domains using the multibox approach with no radial profile variation:

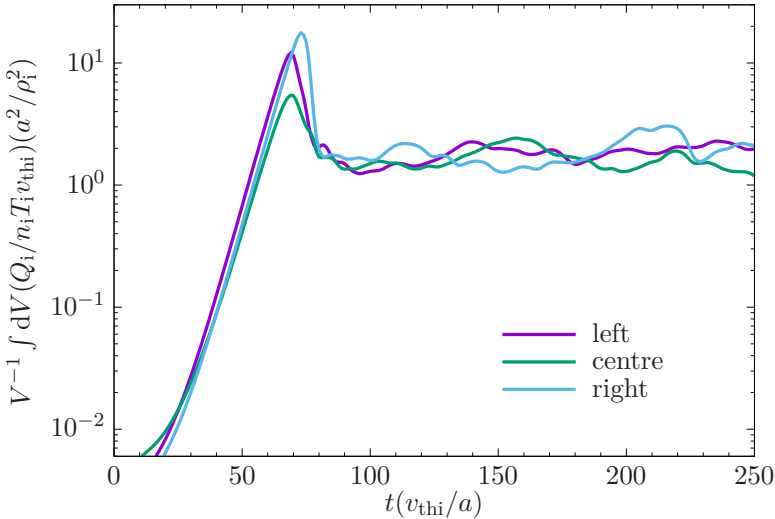

Figure: Ion heat flux for each simulation domain.

SUBSIDIARY EXPANSION: The gyrokinetic parameter, $\rho_* \doteq \rho_\mathrm{i}/a$, is kept small.

Define a new expansion parameter $\Delta = \ell_x/a$, where ℓ_x is the radial width of the simulation.

Using the subsidiary ordering $\rho_* \ll \Delta \ll 1$, expand GKE in Δ to first order. Doing so results in terms such as

$$\mathrm{i}\omega_{\mathrm{D},\boldsymbol{k},s}\left(g_{\boldsymbol{k},s}+\frac{Z_s e}{T_s}F_s J_{0s}\varphi_{\boldsymbol{k}}\right) \approx \left[\mathrm{i}\omega_{\mathrm{D},\boldsymbol{k},s}\left(g_{\boldsymbol{k},s}+\frac{Z_s e}{T_s}F_s J_{0s}\varphi_{\boldsymbol{k}}\right)\right]_{r=r_0}$$
$$+\hat{\mathcal{X}}\left[(\mathrm{i}\omega_{\mathrm{D},\boldsymbol{k},s})'\left(g_{\boldsymbol{k},s}+\frac{Z_s e}{T_s}F_s J_{0s}\varphi_{\boldsymbol{k}}\right)+Z_s e\left(\frac{F_s}{T_s}\right)'\mathrm{i}\tilde{\omega}_{\mathrm{D},\boldsymbol{k},s}J_{0s}\varphi_{\boldsymbol{k}}\right]$$
$$+\mathrm{i}\tilde{\omega}_{\mathrm{D},\boldsymbol{k},s}\hat{\mathcal{X}}\left(\frac{Z_s e}{T_s}F_s J_0'\varphi_{\boldsymbol{k}}\right),$$

red:	full
green:	$\mathcal{O}(1)$
blue:	$\mathcal{O}(\Delta)$

where $\hat{\mathcal{X}}(\cdots) \doteq \mathcal{F}_{\boldsymbol{k}}\left\{(r-r_0)\mathcal{F}_{\boldsymbol{k}}^{-1}\{\cdots\}\right\}$, $\mathcal{F}_{\boldsymbol{k}}$ is the Fourier transform, primes denote differentiation w.r.t r, e.g., $J_0'(a_{\boldsymbol{k},s}) = -(J_{1s}/a_{\boldsymbol{k},s})a_{\boldsymbol{k},s}^2\left[(\ln k_\perp^2)' - (\ln B)'\right]$.

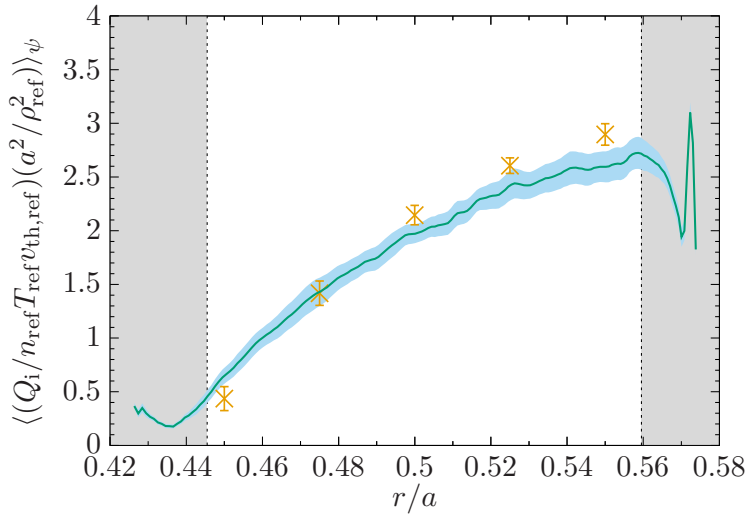

Figure: Radial heat flux profiles for radially global CBC. Orange crosses are generated using local simulations. Grey regions denote boundary regions.

SOURCES & SINKS: Needed to prevent flattening of the background profiles.

Global `Stella` will include two options for sources and sinks:

- Krook-type operator which has become the de facto standard in global gyrokinetics.
- Novel projector approach that is more physically motivated.

Our projector sink/source is enabled by the scale separation of our hybrid approach.
MOTIVATION: Consider a general equation

$$\frac{\partial g}{\partial t} = \Gamma(g),$$

where Γ is a general nonlinear operator. Now consider $\langle g \rangle$, where angular brackets denote some large-scale average, then the equation for $g' = g - \langle g \rangle$ is given by

$$\frac{\partial g'}{\partial t} = \Gamma(g) - \langle \Gamma(g) \rangle.$$

In our system, g represents the distribution function while Γ is the gyrokinetic equation. The operation in red comprises our source/sink.

Our gyrokinetic equation is then

$$\frac{\partial f_s^{\mathrm{tb}}}{\partial t} = -(v_\parallel \hat{\boldsymbol{b}} + \boldsymbol{v}_{\mathrm{D}} + \boldsymbol{v}_E^{\mathrm{lw}} + \boldsymbol{v}_E^{\mathrm{tb}}) \cdot \boldsymbol{\nabla}_{\boldsymbol{R}} f_s^{\mathrm{tb}} + \mu \hat{\boldsymbol{b}} \cdot \boldsymbol{\nabla}_{\boldsymbol{R}} B \frac{\partial f_s^{\mathrm{tb}}}{\partial v_\parallel}$$
$$- \frac{Z_s e f_{\mathrm{Ms}}}{T_s} (v_\parallel \hat{\boldsymbol{b}} + \boldsymbol{v}_{\mathrm{D}} + \boldsymbol{v}_E^{\mathrm{lw}}) \cdot \boldsymbol{\nabla}_{\boldsymbol{R}} \langle \varphi^{\mathrm{tb}} \rangle - \langle \text{all the red terms} \rangle_{\mathrm{T}}$$

where $\langle \cdots \rangle_{\mathrm{T}} = \langle \langle \cdots \rangle_{\boldsymbol{x}_\perp} \rangle_t$ is a 'transport' average that consists of a perpendicular areal average

$$\langle \cdots \rangle_{\boldsymbol{x}_\perp} \doteq \frac{1}{(\ell_x - 2L_{\mathrm{boundary}})\ell_y} \iint (\cdots)\, \mathrm{d}x\, \mathrm{d}y$$

and an exponentially weighted time average

$$\langle \cdots \rangle_t \doteq \frac{\int_0^t \mathrm{d}t' \exp(t'/\tau_{\mathrm{s}})(\cdots)}{\int_0^t \mathrm{d}t' \exp(t'/\tau_{\mathrm{s}})}.$$

This time-averaging procedure is similar to what is currently used in `GYRO`.

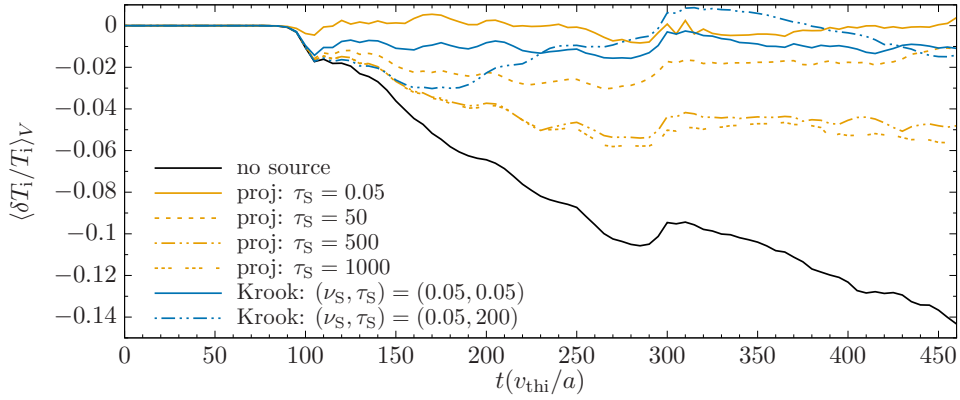

Figure: Evolution of the volume-averaged temperture using both projection (orange) and Krook (blue) operators, as well as without any source (black) for comparison.

Now let's do something interesting! Consider situation where

- Left box is marginally unstable (and possibly in Dimits regime)
- Right box is strongly driven (beyond Dimits)

What happens? Choose $R/L_{\mathrm{T}} = 5.0$ for the center box.

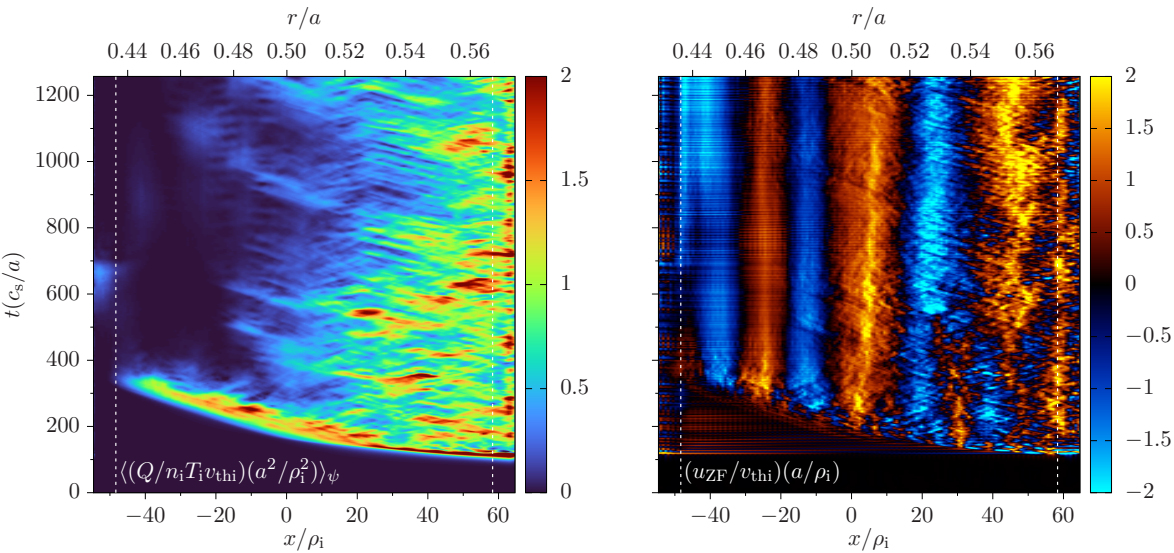

Figure: Heat flux (left) and zonal flow velocity (right) as a function of radius (horizontal axis) and time (vertical axis). White dashed lines denote boundaries.

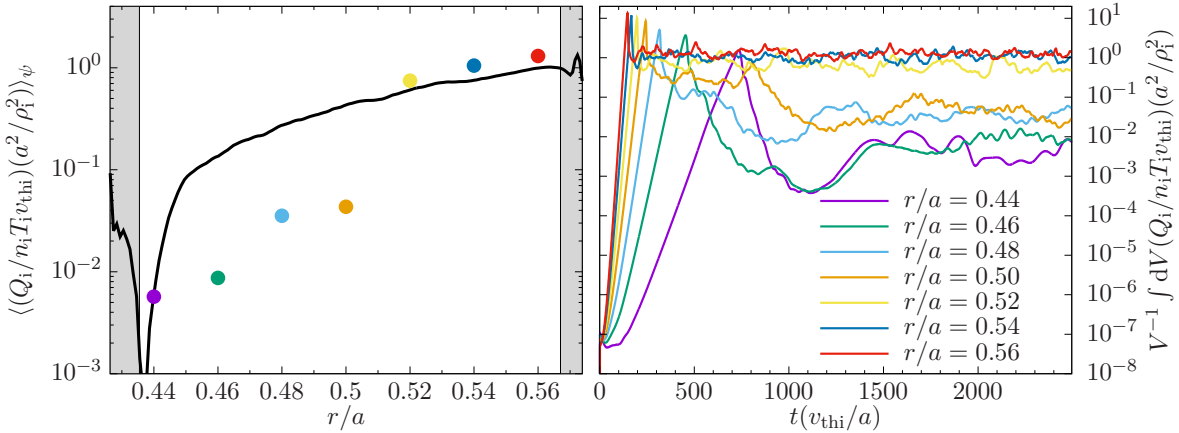

Figure: *left:* Time averaged heat fluxes, including global and local simulations. *right:* Total heat flux versus time for local simulations spread over the previous radial domain.

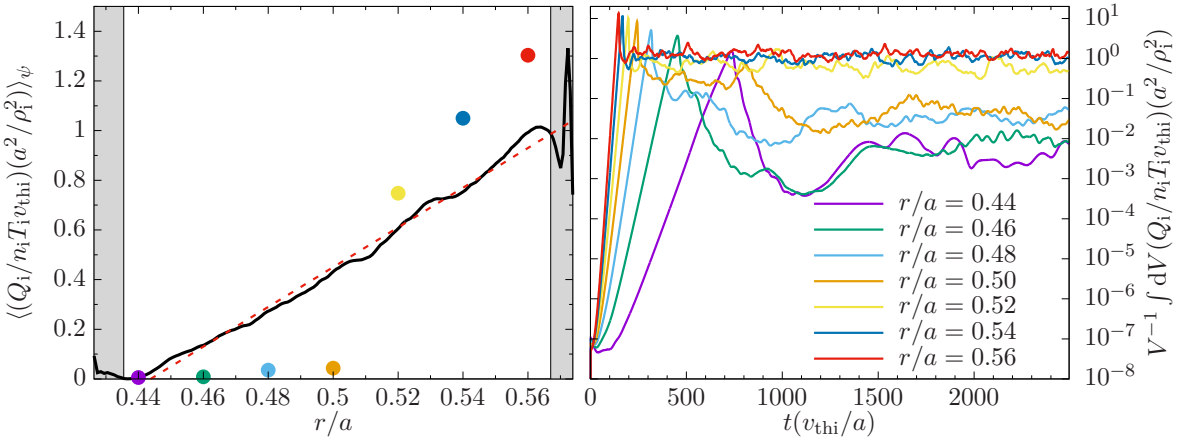

Figure: *left:* Time averaged heat fluxes, including global and local simulations. *right:* Total heat flux versus time for local simulations spread over the previous radial domain.

Radial variation introduces symmetry breaking that can lead to flux of parallel momentum.

- why is it negative?
- what is its radial profile?

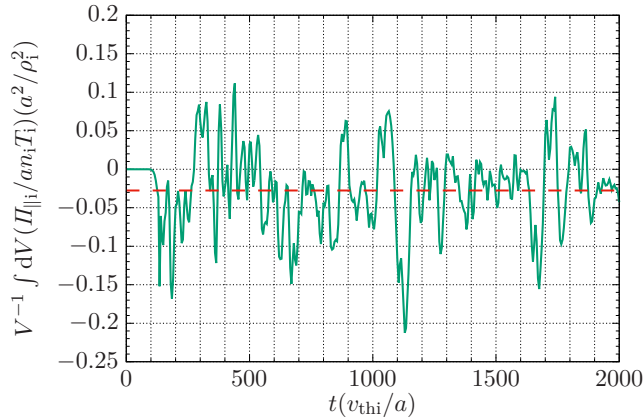

Figure: Parallel momentum flux over time for CBC. Dashed line denotes time average.

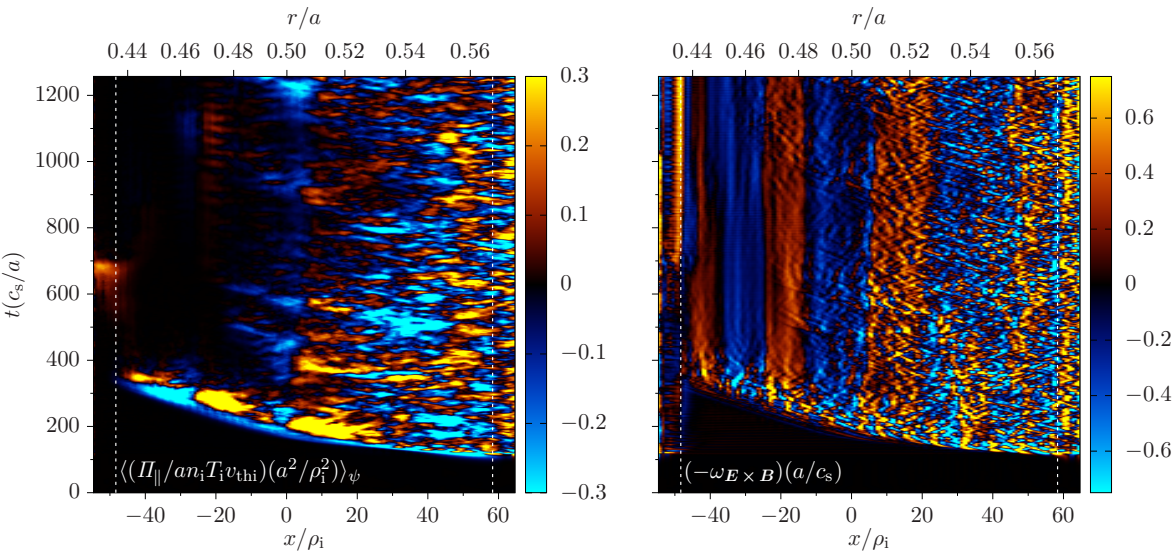

Figure: Parallel momentum flux (left) and zonal flow shear (right) as a function of radius (horizontal axis) and time (vertical axis). White dashed lines denote boundaries. $\boldsymbol{E}\times\boldsymbol{B}$ shear rate has been filtered to remove small-scale fluctuations.

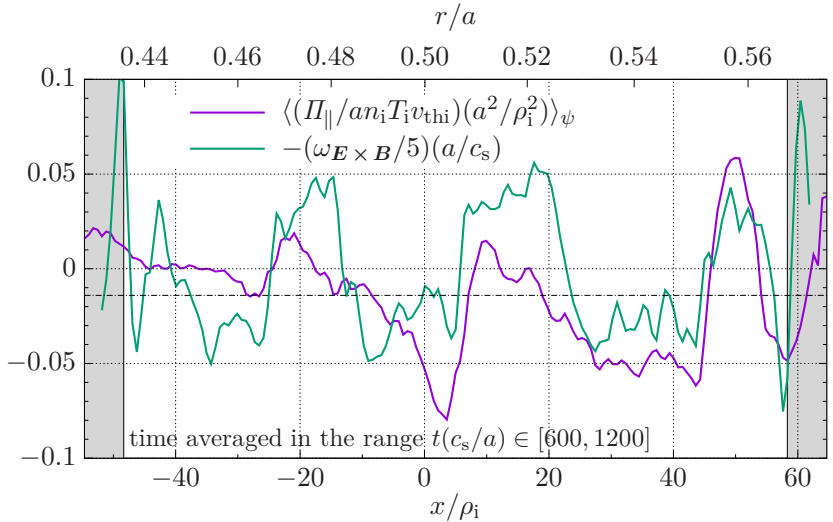

Figure: Time-averaged parallel momentum flux (purple line) and $\boldsymbol{E}\times\boldsymbol{B}$ shear rate (green line) as a function of radius. The latter has been filtered to remove small-scale fluctuations. Dashed dotted line denotes average of momentum flux. Grey regions denote boundary regions.

TECHNICAL DETAILS

A NOTE ON DEALIASING:

Convolutions are performed pseudo-spectrally by transforming to real space.

Nonlinearities (*local*):

- convolution of $\varphi_{\boldsymbol{k}}$ with $g_{\boldsymbol{k},s}$

Radial variation terms (*global*):

- convolution of $r - r_0$ with other terms

2/3^{rds} dealiasing does not work for the radial variation terms!

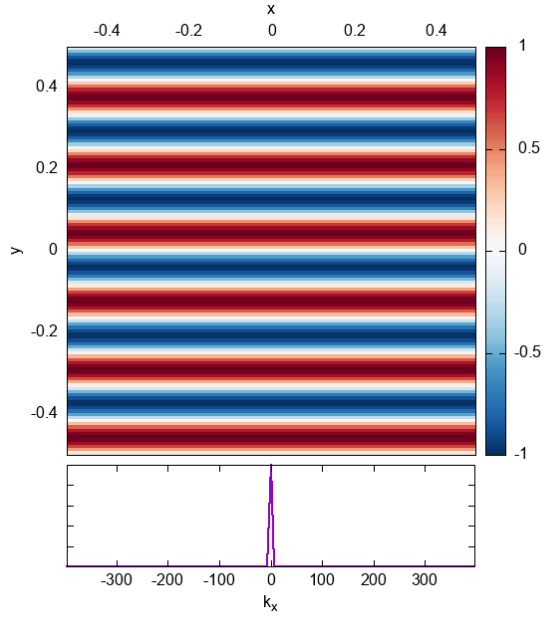

A NOTE ON DEALIASING:

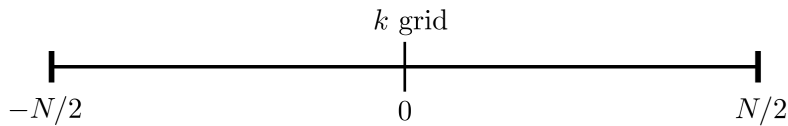

Figure: Wavenumber diagram of the $2/3^{\mathrm{rds}}$ dealiasing rule. When information falls out of the wavenumber grid, it gets down or upsampled by N until it falls within the grid.

A NOTE ON DEALIASING:

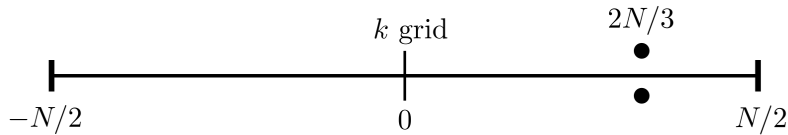

Figure: Wavenumber diagram of the $2/3^{\mathrm{rds}}$ dealiasing rule. When information falls out of the wavenumber grid, it gets down or upsampled by N until it falls within the grid.

A NOTE ON DEALIASING:

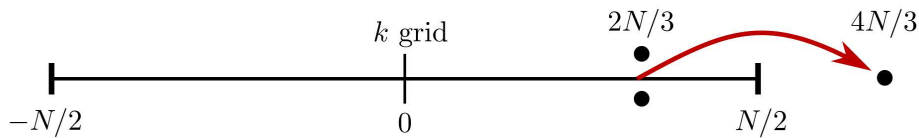

Figure: Wavenumber diagram of the $2/3^{\text{rds}}$ dealiasing rule. When information falls out of the wavenumber grid, it gets down or upsampled by N until it falls within the grid.

A NOTE ON DEALIASING:

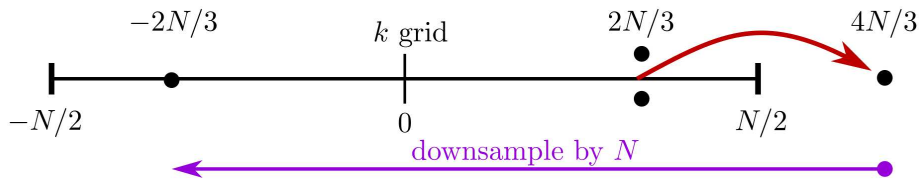

Figure: Wavenumber diagram of the $2/3^{\text{rds}}$ dealiasing rule. When information falls out of the wavenumber grid, it gets down or upsampled by N until it falls within the grid.

A NOTE ON DEALIASING:

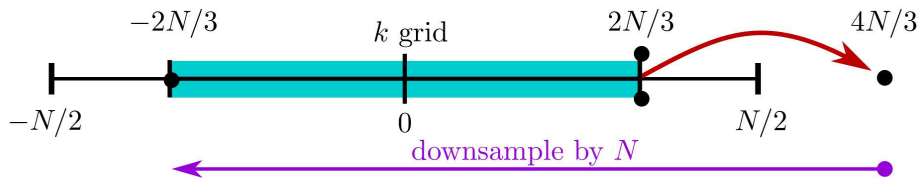

Figure: Wavenumber diagram of the $2/3^{\text{rds}}$ dealiasing rule. When information falls out of the wavenumber grid, it gets down or upsampled by N until it falls within the grid.

A NOTE ON DEALIASING:

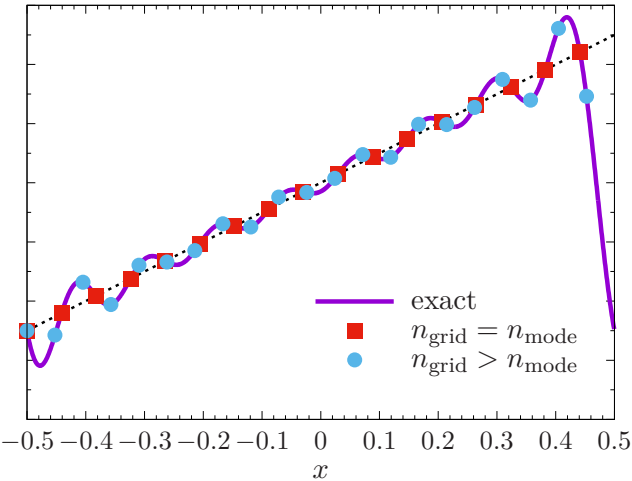

Figure: A demonstration of why the non-periodic linear function x cannot be truncated. The linear function here is truncated to 17 modes (red squares), which results in the purple line. If these modes are transformed to a higher resolution grid, the blue circles result.

Instead of $2/3^{\mathrm{rds}}$ dealiasing, we use the smallness of profile shearing ($\sim\rho_*$, not $\sim\Delta$) and rely solely on hyperdissipation.

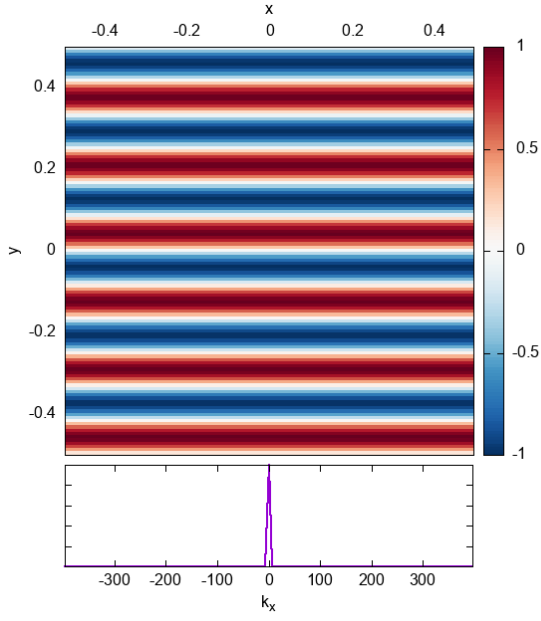

GLOBALISING MILLER: The geometrical coefficients for local simulation are calculated using the Miller equilibrium,

$$R(r,\theta) = R_0(r) + r\cos[\theta + \sin\theta \arcsin\delta(r)],$$
$$Z(r,\theta) = \kappa(r) r \sin(\theta),$$

along with the Grad-Shafranov equation,

$$R^2 \boldsymbol{\nabla}\cdot\left(\frac{\boldsymbol{\nabla}\psi}{R^2}\right) = -4\pi R^2 \frac{\mathrm{d}p}{\mathrm{d}\psi} - I\frac{\mathrm{d}I}{\mathrm{d}\psi},$$

locally around a flux surface. Here, $I = B_{\mathrm{T}} R$.

To globalise, one cannot simply solve Grad-Shafranov at various radial locations!

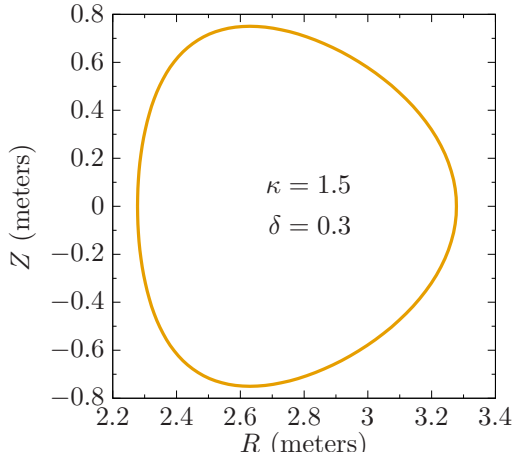

Figure: Miller equilibrium with triangularity $\delta = 0.3$ and elongation $\kappa = 1.5$.

GLOBALISING MILLER: Manipulating the Grad-Shafranov equation results in

$$\frac{I'}{I}\int_0^{2\pi}\mathrm{d}\theta\,\frac{\mathcal{J}_r}{R^2}\left(1+\frac{I^2}{|\boldsymbol{\nabla}\psi|^2}\right)=-\int_0^{2\pi}\mathrm{d}\theta\Bigg(\frac{4\pi\mathcal{J}_r}{|\boldsymbol{\nabla}\psi|^2}p'-\frac{\mathcal{J}_r}{R^2}\left(\frac{q'}{q}+\frac{2R'}{R}\right)$$
$$+\frac{1}{|\boldsymbol{\nabla}r|^2}\left\{\frac{1}{\mathcal{J}_r}\left[\left(\frac{\partial Z}{\partial\theta}\right)^2+\left(\frac{\partial R}{\partial\theta}\right)^2\right]'-\frac{\partial r_z}{\partial\theta}\right\}\Bigg).$$

where $\mathcal{J}_r$ is the Jacobian in (r,θ,ζ) coordinates. Similar equations for $\mathcal{J}_r$ and $(|\boldsymbol{\nabla}\psi|^2)'$ can be derived. For global `stella`, we calculate the derivative of these equations, which results in equations like

$$\frac{\mathcal{J}_r'}{R}=\frac{\mathcal{J}_rR'}{R^2}+R''\frac{\partial Z}{\partial\theta}+R'\frac{\partial Z'}{\partial\theta}-Z''\frac{\partial R}{\partial\theta}-Z'\frac{\partial R'}{\partial\theta}.$$

We specify as input β'', ψ'', q''. We cannot self-consistently specify higher derivatives of δ and κ, so we must use additional constraints on R'' and Z''.

QUASINEUTRALITY: The electrostatic potential φ is determined using quasineutrality,

$$\Theta(r_0)\varphi_{\boldsymbol{k}} + \hat{\mathcal{X}}\left(\Theta'\varphi_{\boldsymbol{k}}\right) = \frac{2}{\pi^{1/2}} \sum_s Z_s \int \mathrm{d}v_{\parallel} \int \mathrm{d}\mu\, B(r) J_{0s}(k_\perp v_\perp/\Omega_s) g_{\boldsymbol{k},s},$$

where $\boldsymbol{k}$ is the wavenumber and

$$\Theta = \sum_s \int \mathrm{d}v^3\, Z_s^2 e (1 - J_{0s}^2) \frac{F_s}{T_s},$$

$$\Theta' = \sum_s \int \mathrm{d}v^3\, Z_s^2 e \left[(1 - J_{0s}^2) \left(\frac{F_s}{T_s}\right)' + 2 J_{0s} J_{1s} \left(\frac{k_\perp v_\perp}{\Omega_s}\right)' \frac{F_s}{T_s} \right].$$

However, $1 - \Gamma_{0s} \to 0$ as $k_\perp \to 0$.

- For non-zonal modes, quasineutrality is solved iteratively for φ with the blue terms treated as small.
- For zonal modes, the entire LHS must be inverted.

PARALLEL BOUNDARY CONDITION: (Beer *et al.* 1995 PoP)

$$A(\psi, \alpha(\psi, \zeta, \theta = 0), \theta = 0) = A(\psi, \alpha(\psi, \zeta, \theta = 2\pi N), \theta = 2\pi N),$$

where $\alpha = \zeta - q(\psi)\theta$. In Fourier space, with ψ as radial coordinate,

$$\sum_{k_\psi, k_\alpha} A_{\boldsymbol{k}}(\theta = 0) \mathrm{e}^{\mathrm{i}k_\psi(\psi - \psi_0) + \mathrm{i}k_\alpha \alpha} =$$

$$\sum_{k_\psi, k_\alpha} A_{\boldsymbol{k}}(\theta = 2\pi) \mathrm{e}^{\mathrm{i}k_\psi(\psi - \psi_0) + \mathrm{i}k_\alpha \alpha - 2\pi N \mathrm{i}k_\alpha [q_0 + q'(\psi - \psi_0) + q''(\psi - \psi_0)^2/2 + \ldots]}.$$

Problems if q'', q''', $\ldots \neq 0$. Instead, use q as the radial coordinate:

$$\sum_{k_q, k_\alpha} A_{\boldsymbol{k}}(\theta = 0) \mathrm{e}^{\mathrm{i}k_q(q - q_0) + \mathrm{i}k_\alpha \alpha} = \sum_{k_q, k_\alpha} A_{\boldsymbol{k}}(\theta = 2\pi) \mathrm{e}^{\mathrm{i}(k_q - 2\pi N k_\alpha)(q - q_0) + \mathrm{i}k_\alpha \alpha - 2\pi N \mathrm{i}k_\alpha q_0},$$

and so now

$$A_{k_q, k_\alpha}(\theta = 0) = C_k A_{k_q + \Delta k_q, k_\alpha}(\theta = 2\pi),$$

where $C_k = \exp(-2\pi N \mathrm{i}k_\alpha q_0)$ and $\Delta k_q = 2\pi N k_\alpha$.

THE $k_\perp = 0$ MODE:

Hidden inside the gyrokinetic equation is a drift-kinetic equation for the $\boldsymbol{k}_\perp = 0$ mode. In the local limit, this equation is

$$\frac{\partial g_{\boldsymbol{k}=0,s}}{\partial t} + v_\parallel \left(\hat{\boldsymbol{b}} \cdot \boldsymbol{\nabla} g_{\boldsymbol{k}=0,s} + \frac{Z_s e}{T_s} F_s \hat{\boldsymbol{b}} \cdot \boldsymbol{\nabla} \varphi_{\boldsymbol{k}=0} \right) - \frac{\mu_s}{m_s} \hat{\boldsymbol{b}} \cdot \boldsymbol{\nabla} B \frac{\partial g_{\boldsymbol{k}=0,s}}{\partial v_\parallel} = 0.$$

As the nonlinearity does not appear here, this does not couple to the rest of the GKE. However, this independence is broken in our subsidiary expansion.
This mode consists of two pieces, one for $g_{\boldsymbol{k},s}$ and $\varphi_{\boldsymbol{k}}$.

- The $g_{\boldsymbol{k},s}$ portion comes about from the mismatch of fluxes between the radial boundaries — natural outcome of the new BCs
- The $\varphi_{\boldsymbol{k}}$ portion which gives the parallel electric field $E_\parallel$ is more subtle... *and much more difficult to deal with!*

THE $k_\perp = 0$ ELECTROSTATIC POTENTIAL ($E_\parallel$): KINETIC SPECIES

For $\boldsymbol{k}_\perp = \boldsymbol{0}$, $J_{0s}^2 - 1 = J_{1s} = 0$, or in other words, $\langle\varphi\rangle = \varphi$.

For kinetic species, the quasineutrality equation is

$$\Theta(r_0)\varphi_{\boldsymbol{k}} + \hat{\mathcal{X}}\left(\Theta'\varphi_{\boldsymbol{k}}\right) = \frac{2}{\pi^{1/2}}\sum_s Z_s \int \mathrm{d}v_\parallel \int \mathrm{d}\mu\, B(r) J_{0s}(k_\perp v_\perp/\Omega_s) g_{\boldsymbol{k},s},$$

NB: $\Theta\varphi_{\boldsymbol{k}=\boldsymbol{0}} = \Theta'\varphi_{\boldsymbol{k}=\boldsymbol{0}} = 0$ *— zero mode does not appear!*
Rather, we instead have a solvability condition: taking the local limit of the quasineutrality equation, along with

$$\frac{\partial g_{\boldsymbol{k}=0,s}}{\partial t} + v_\parallel\left(\hat{\boldsymbol{b}}\cdot\boldsymbol{\nabla} g_{\boldsymbol{k}=0,s} + \frac{Z_s e}{T_s}F_s\hat{\boldsymbol{b}}\cdot\boldsymbol{\nabla}\varphi_{\boldsymbol{k}=0}\right) - \frac{\mu_s}{m_s}\hat{\boldsymbol{b}}\cdot\boldsymbol{\nabla}B\frac{\partial g_{\boldsymbol{k}=0,s}}{\partial v_\parallel} = 0,$$

by $\perp$-areal averaging and combining, we get $\langle\sum_s Z_s\int \mathrm{d}^3v\, v_\parallel \hat{\boldsymbol{b}}\cdot\boldsymbol{\nabla} g_{\boldsymbol{k}=0,s}\rangle_{\boldsymbol{x}_\perp} = 0$ and

$$\left\langle \sum_s Z_s \int \mathrm{d}^3v\, v_\parallel \hat{\boldsymbol{b}}\cdot\boldsymbol{\nabla}\left[v_\parallel\left(\hat{\boldsymbol{b}}\cdot\boldsymbol{\nabla} g_{\boldsymbol{k}=0,s} + \frac{Z_s e}{T_s}F_s\hat{\boldsymbol{b}}\cdot\boldsymbol{\nabla}\varphi_{\boldsymbol{k}=0}\right) - \frac{\mu_s}{m_s}\hat{\boldsymbol{b}}\cdot\boldsymbol{\nabla}B\frac{\partial g_{\boldsymbol{k}=0,s}}{\partial v_\parallel}\right]\right\rangle_{\boldsymbol{x}_\perp} = 0.$$

Parallel physics determines this mode.

THE $\boldsymbol{k}_\perp = 0$ ELECTROSTATIC POTENTIAL ($E_\parallel$): KINETIC SPECIES

For $\boldsymbol{k}_\perp = \boldsymbol{0}$, $J_{0s}^2 - 1 = J_{1s} = 0$, or in other words, $\langle\varphi\rangle = \varphi$.

For kinetic species, the quasineutrality equation is (*local limit*)

$$\cancel{\left\langle \Theta(r_0)\varphi_{\boldsymbol{k}} + \hat{\mathcal{X}}(\Theta'\varphi_{\boldsymbol{k}}) \right\rangle_{\boldsymbol{x}_\perp}^{0}} = \left\langle \frac{2}{\pi^{1/2}} \sum_s Z_s \int \mathrm{d}v_\parallel \int \mathrm{d}\mu\, B g_{\boldsymbol{k}=0,s} \right\rangle_{\boldsymbol{x}_\perp},$$

NB: $\Theta\varphi_{\boldsymbol{k}=\boldsymbol{0}} = \Theta'\varphi_{\boldsymbol{k}=\boldsymbol{0}} = 0$ — *zero mode does not appear!*
Rather, we instead have a solvability condition: taking the local limit of the quasineutrality equation, along with

$$\frac{\partial g_{\boldsymbol{k}=0,s}}{\partial t} + v_\parallel \left(\hat{\boldsymbol{b}}\cdot\boldsymbol{\nabla} g_{\boldsymbol{k}=0,s} + \frac{Z_s e}{T_s} F_s \hat{\boldsymbol{b}}\cdot\boldsymbol{\nabla}\varphi_{\boldsymbol{k}=0} \right) - \frac{\mu_s}{m_s}\hat{\boldsymbol{b}}\cdot\boldsymbol{\nabla}B\frac{\partial g_{\boldsymbol{k}=0,s}}{\partial v_\parallel} = 0,$$

by $\perp$-areal averaging and combining, we get $\langle \sum_s Z_s \int \mathrm{d}^3v\, v_\parallel \hat{\boldsymbol{b}}\cdot\boldsymbol{\nabla} g_{\boldsymbol{k}=0,s}\rangle_{\boldsymbol{x}_\perp} = 0$ and

$$\left\langle \sum_s Z_s \int \mathrm{d}^3v\, v_\parallel \hat{\boldsymbol{b}}\cdot\boldsymbol{\nabla} \left[v_\parallel \left(\hat{\boldsymbol{b}}\cdot\boldsymbol{\nabla} g_{\boldsymbol{k}=0,s} + \frac{Z_s e}{T_s} F_s \hat{\boldsymbol{b}}\cdot\boldsymbol{\nabla}\varphi_{\boldsymbol{k}=0} \right) - \frac{\mu_s}{m_s}\hat{\boldsymbol{b}}\cdot\boldsymbol{\nabla}B\frac{\partial g_{\boldsymbol{k}=0,s}}{\partial v_\parallel} \right] \right\rangle_{\boldsymbol{x}_\perp} = 0.$$

Parallel physics determines this mode.

THE $k_\perp = 0$ ELECTROSTATIC POTENTIAL ($E_\parallel$): ADIABATIC ELECTRONS

Things are somewhat easier with adiabatic electrons... quasineutrality has parallel physics is already built-in:

$$\int \mathrm{d}^3v\, J_{0s} g_{\boldsymbol{k},s} - \Theta(r)\varphi_{\boldsymbol{k}} = \frac{n_\mathrm{e}}{T_\mathrm{e}} \left(\varphi_{\boldsymbol{k}} - \langle \varphi_{\boldsymbol{k}} \rangle_\psi\right).$$

Now $\varphi_{\boldsymbol{k}=\boldsymbol{0}}$ appears on the RHS. We still have a solvability condition,

$$\left\langle \int \mathrm{d}^3v\, J_{0s} g_{\boldsymbol{k},s} - \Theta(r)\varphi_{\boldsymbol{k}} \right\rangle_\psi = 0,$$

which is broken by the radial BCs. In global `stella`, we employ a small correction term to fix this:

$$\int \mathrm{d}^3v\, J_{0s} g_{\boldsymbol{k},s} - \Theta(r)\varphi_{\boldsymbol{k}} - \left\langle \left\langle \int \mathrm{d}^3v\, J_{0s} g_{\boldsymbol{k},s} - \Theta(r)\varphi_{\boldsymbol{k}} \right\rangle_\psi \right\rangle_{\boldsymbol{x}_\perp} = \frac{n_\mathrm{e}}{T_\mathrm{e}} \left(\varphi_{\boldsymbol{k}} - \langle \varphi_{\boldsymbol{k}} \rangle_\psi\right).$$

With this correction, all that's needed is a gauge condition (we use $\varphi_{\boldsymbol{k}=\boldsymbol{0}} = 0$ at the inboard midplane).

PLANS FOR EXTENDING THE `stella` CODE

Some novel current and planned features of `stella`:

- ✓ Full-flux surface `stella` for stellarators
- ✓ Response matrix methods are hybridized using shared memory — *faster LU decompositions and larger matrices*
  - ⏳ Shared memory hybridization will be applied to all of `stella` — *scaling to 100s of thousands of cores*
- ⏳ LU decomposition coupled with global QN solver — *global-local simulations with implicit electrons*
- ⏳ Electromagnetic effects in `stella` — *global-local electromagnetic simulations*

Stay tuned for these exciting developments!

SUMMARY:

- Global `stella` offers a complimentary approach to global gyrokinetics
- Multiple-flux-tube method performs robustly under a variety of configurations

FUTURE STEPS:

- In-depth study of intrinsic rotation generation
- Determine how turbulence spreading plays out
- Investigate bistable states recently discovered by Christen 2021
- Apply this method to physically relevant profiles near the pedestal

Thank you for listening!